International Journal of Engineering Trends and Technology
ISSN: 2231–5381 / https://doi.org/10.14445/22315381/IJETT-V72I5P124

Volume 72 Issue 5, 232-242, May 2024

Original Article

Performance Enhancement of Dual Active Full-Bridge Converter with Advanced Control Modules for V2G and G2V Application

Ramesh Jatoth[1], B. Mangu[2]

[1,2]*Department of Electrical Engineering, University College of Engineering(A),OU, Hyderabad.*

[1]*Corresponding Author : ramesh.jatoth@gmail.com*

Received: 26 December 2023 Revised: 07 April 2024 Accepted: 15 April 2024 Published: 26 May 2024

Abstract *- The use of Electric Vehicles (EVs) for domestic transportation is increasing rapidly. As a result, more charging stations are needed to meet the demand for charging EV batteries. To achieve efficient power transfer, a Dual Active Full-Bridge topology (DAFB) is integrated into the charging module, which can exchange power bi-directionally. The charging module can charge or discharge the EV battery as required in V2G and G2V modes. The adopted phase shift modulation (PSM) control structure for controlling the DAFB switches is updated with advanced controllers of Fuzzy, ANFIS, or DSM-PI. A comparative analysis is conducted on different controllers operated with variable reference set points to determine the best controller module. The proposed topology with advanced controllers is analyzed on a grid distribution network with a Photo Voltaic (PV) plant integrated for renewable power sharing, charging the EV battery. The test system is designed in MATLAB. Simulink software is used for modeling and analysis, generating comparative graphs to validate the results.*

Keywords *- ANFIS (Adaptive-Neuro Fuzzy Inference System), DAFB (Dual Active Full Bridge), DSM-PI (Dual Sliding Mode – Proportional Integral), EV (Electric Vehicle), FIS (Fuzzy Inference System), G2V (Grid to Vehicle), MATLAB (Matrix Laboratory), PSM (Phase shift modulation), PV (Photo Voltaic), Simulink, V2G (vehicle to grid).*

1. Introduction

Due to the increase in global warming and natural disasters, it is important to reduce emissions from vehicles transportation that are used for commercial and domestic purposes [1]. There is much research being done on Electric Vehicle (EV) technology to replace traditional fossil fuel combustion vehicles. EVs use a battery unit that stores specific electrical power for driving. The batteries of these EVs can be charged from charging stations or a regular grid on a domestic power rating, and these charging methods are divided into DC charging and AC charging [2]. DC charging has more power than AC charging because the DC charging station is supplied from a 3-phase grid. AC charging, on the other hand, has lower power because only a 1-phase supply can be used in domestic electrical connections. Due to the advantages provided by DC charging stations, it is recommended that EV batteries are charged from DC plug-in charging locations. DC charging stations are connected directly to the distribution lines (11kV) at optimal locations. A step-down load transformer transfers power to the DC charging module at load voltage magnitude levels [3]. Charging modules convert the 3-phase AC voltages from the transformer to higher power DC voltage. Later on, this voltage is stabilized by different DC-DC converters to charge the EV battery. These converters can either be unidirectional or bidirectional, depending on the requirement. The unidirectional converter only charges the battery, represented as the Grid to Vehicle (G2V) [4]. The bidirectional converter can also inject power into the grid, represented as a Vehicle to the Grid (V2G). By installing a bidirectional converter, the charging module will have the added advantage of injecting power into the grid from the EV battery when needed.

Most of the research for bidirectional power exchange uses a conventional basic two-switch DC-DC buck-boost converter. However, this basic converter has drawbacks, such as lower efficiency and higher DC voltage ripple content, which can be a greater disadvantage for charging high-rating EV batteries. The conventional bidirectional converter has also had more power loss which impacts the efficiency of the system. This converter may damage the EV battery, and it can also inject huge harmonics into the grid. Therefore, the basic converter is replaced by the Dual Active Full Bridge (DAFB) converter, which has very low operating voltage ripple and high efficiency, even during higher power transfer conditions [5]. The DAFB circuit topology is considered to be the most ideal selection for G2V and V2G operating modes in the system.

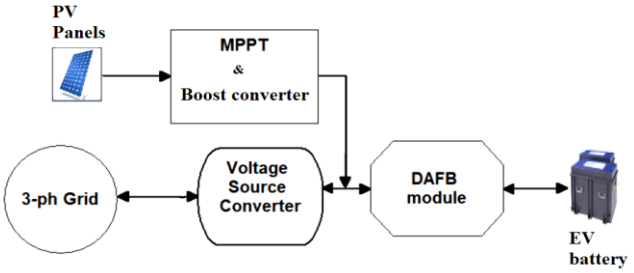

Fig. 1 Test system network with DAFB module

The Figure 1 test system network contains a PV source for renewable power sharing. The PV module has a Beta (β) MPPT method that extracts maximum power from PV panels connected to a boost converter [6]. The EV battery can be charged using power from the PV module or the 3-ph grid, depending on the solar irradiation availability. The EV charging station consists of a Voltage Source Converter (VSC), DAFB, and EV battery [7]. The VSC is a bidirectional converter that can function as a rectifier and inverter in the G2V and V2G modes, respectively. The DAFB uses the phase shift pulse modulation (PSPM) technique to charge and discharge the EV battery. The PSPM technique is controlled by feedback loop control with different controllers for better stability of DAFB topology [8]. The charging and discharging of the battery can be controlled by voltage or current reference feedback. In this paper, Section I introduces the proposed test network and the modules PV source and EV charging station. Section II describes the configuration of the DAFB module and the design of the PSPM technique for controlling battery charge and discharge. Section III covers different controllers, including Proportional-Integral (PI), Fuzzy Inference System (FIS), Adaptive-Neuro Fuzzy Inference System (ANFIS), and Dual Sliding Mode-PI (DSM-PI) modeling and design [9] [10]. The results obtained with different controllers and references are discussed and validated in Section IV. Finally, Section V concludes the paper by determining the best controller with parametric comparative results, followed by references.

2. DAFB Configuration

The DAFB circuit topology is widely recognized as the most efficient bidirectional DC-DC converter for applications with higher power ratings [11] [12]. It is primarily used in systems where bidirectional operation is essential and where the power direction is changed as per the requirement. The DAFB converter is a combination of two full bridges, with each bridge consisting of four IGBT switches. These bridges are magnetically coupled by a High-Frequency Transformer (HFTF) that transfers power from one network to the other. The full bridges are operated with high-frequency pulse signals that convert DC-AC-DC [13]. One of the full bridges works as an inverter, and the other works as a rectifier, which is determined by the direction of operation. The circuit configuration diagram of the DAFB converter is shown in Figure 2 below.

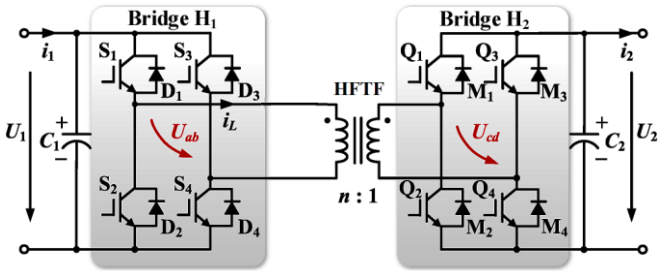

Fig. 2 DAFB circuit configuration

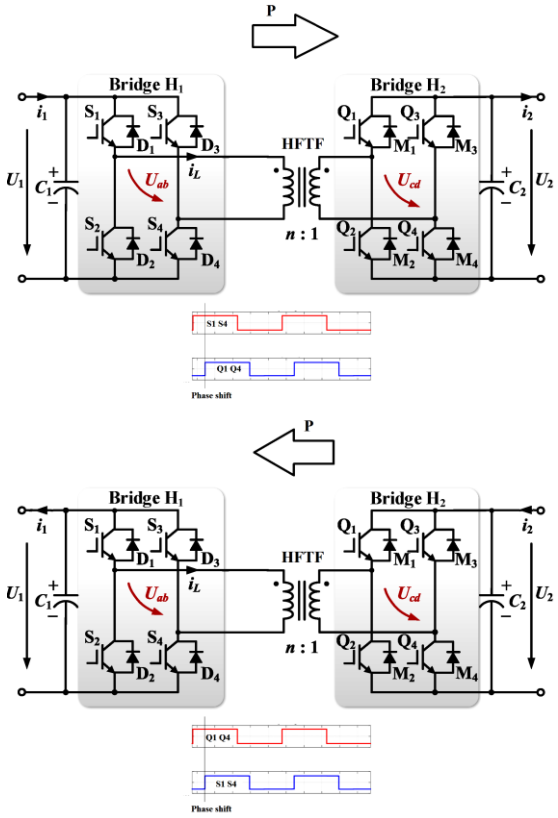

Fig. 3 DAFB circuit power transfer modes

As per Figure 2, the bridge on the primary side of HFTF comprises switches S1-S4, and switches on the secondary side bridge are Q1-Q4 [14]. The primary side DC voltage and current are U1 and i1, secondary side voltage and current are U2 and i2, respectively. The currents of the proposed topology are given as

$$i_1 = \frac{U_1+nU_2}{R}d + \frac{U_1-nU_2}{R}(1-d) + \frac{L}{RT}\left(I_1 + \frac{U_1+nU_2}{R}\right)\left(e^{-\left(\frac{R}{L}\right)dT} - 1\right) + \frac{L}{RT}\left(\frac{U_1-nU_2}{R} - I_2\right)\left(e^{-\left(\frac{R}{L}\right)(T-dT)} - 1\right) \quad (1)$$

$$i_2 = -\frac{nU_1+n^2U_2}{R}d + \frac{nU_1-n^2U_2}{nR}(1-d) - \frac{L}{RT}\left(nI_1 + \frac{nU_1+n^2U_2}{R}\right)\left(e^{-\left(\frac{R}{L}\right)dT} - 1\right) + \frac{L}{RT}\left(\frac{nU_1-n^2U_2}{R} - nI_2\right)\left(e^{-\left(\frac{R}{L}\right)(T-dT)} - 1\right) \quad (2)$$

In this context, L, R, and T refer to inductance, resistance, and sample time, respectively. The duty ratio of the switches is represented by 'd'. Both bridges utilize a fixed duty ratio of 50% and a fixed switching frequency of 50kHz [15]. The magnitude of the transferring current is controlled using the Phase Shift Pulse Modulation (PSPM) technique, which varies the pulse phase angle. The receiving bridge always has a lagging phase shift (φ) from the other bridge, making it function as a rectifier while the sending bridge serves as an inverter [16]. Figure 3 illustrates the DAFB power flow diagram based on the phase shift of the pulses. The power transfer (P) of the circuit topology with respect to phase shift angle is given as

$$P = \frac{U_1^2}{wL}.\frac{U_2}{N.V_i}\left(1 - \frac{|\varphi|}{\pi}\right) \quad (3)$$

Here, 'w' is the switching frequency (2π*20000), and N is the turns ratio of HFTF. It is possible to control the amount of current being transferred by adjusting the phase shift (φ) of the receiving bridge. When the lagging pulse phase shift is increased, the transferring current magnitude also increases. By controlling the phase shift angle (φ) of the receiving bridge, the current magnitude can be set to any desired reference value. This phase shift angle (φ) is determined by current-oriented feedback control, where the magnitude of the EV battery's charging or discharging current is controlled using the PSPM technique [13]. Figure 4 illustrates the simple structure of PSPM with current reference feedback. In Figure 4, the reference battery current, Ibat ref, is compared to the IB generating current error, which is fed to the phase shift control module [18]. This module comprises different controllers that generate a phase shift angle for the pulses of the receiving power full bridge. The phase shift is adjusted based on the response of the circuit topology for the given reference. The selection of the phase shift on the bridge is determined by the V2G or G2V mode. Several advanced control modules are considered for the generation of the phase shift angle with respect to current error, such as the PI, FIS, ANFIS, and DSM-PI controllers. Each of these controllers has its pros and cons that affect the battery current. The modeling and design of these controllers are discussed in the next section, with tools taken from MATLAB software.

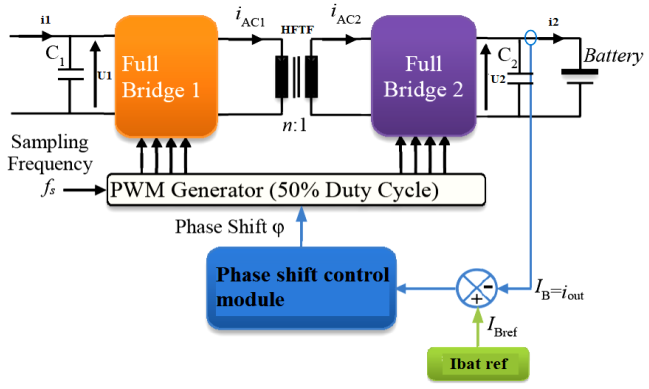

Fig. 4 PSPM control structure

3. Controller Design and Modeling

As per the given system, DAFB is controlled with battery current feedback. The EV battery needs to be charged with a constant current input, which most charging station topologies consider as a reference. This approach makes the battery charge stable power, increasing its reliability and charging speed compared to conventional methods. The charging process is controlled through constant current-oriented feedback control, which adjusts the phase shift angle to achieve the set reference point. In traditional methods, a phase shift control module is included with a PI controller, where the Kp and Ki gains are tuned based on the system response, converting phase angle into time through simulations. The conventional PI controller module is updated with FIS, ANFIS, and DSM-PI controllers, and their designs are further discussed.

3.1. FIS (Fuzzy Inference System)

The FIS controller uses a fuzzy logic tool to implement the change in the phase shift angle of the bridge based on the current error generated. The structure considered for the FIS is the 'mamadani' available in the tool. The FIS controller has one output variable and two input variables [19]. The output variable considered is the phase shift angle (φ), while the input variables are the current error (Ie) and change in current error (dIe). Each variable has seven membership functions in a specific range based on the input reference value (Ibat ref). The input membership functions are taken as a 'gauss' type to cover a larger range, while the output is taken as a 'triangular' type for increased accuracy [20]. The membership functions of the variables in the fuzzy tool are shown in Figure 5. Each membership function of a variable is defined with the specific name given as ZE (Zero), PS (Positive Small), PM (Positive Medium), PB (Positive Big), Negative Small (NS), NM (Negative Medium), NB (Negative Big). The input variable 'Ie' range is set between -100 to 100, the input variable 'dIe' is set between -1 to 1, and the output variable 'φ' is set between -50 to 50 degrees. The output variable 'φ' generates value as per the given 49 rule Table 1.

Based on the input values provided to the Fuzzy Inference System (FIS) within a specific range of the seven membership functions, the output variable is altered. Additionally, the time delay block is given a phase shift 'φ' to introduce a delay in the pulses according to the current error (Ie) generated.

Table 1. Rule table (7x7)

cee	NB	NM	NS	ZE	PS	PM	PB
NB	NB	NB	NB	NB	NM	NS	ZE
NM	NB	NB	NB	NM	NS	ZE	PS
NS	NB	NB	NM	NS	ZE	PS	PM
ZE	NB	NM	NS	ZE	PS	PM	PB
PS	NM	NS	ZE	PS	PM	PB	PB
PM	NS	Z	PS	PM	PB	PB	PB
PB	Z	PS	PM	PB	PB	PB	PB

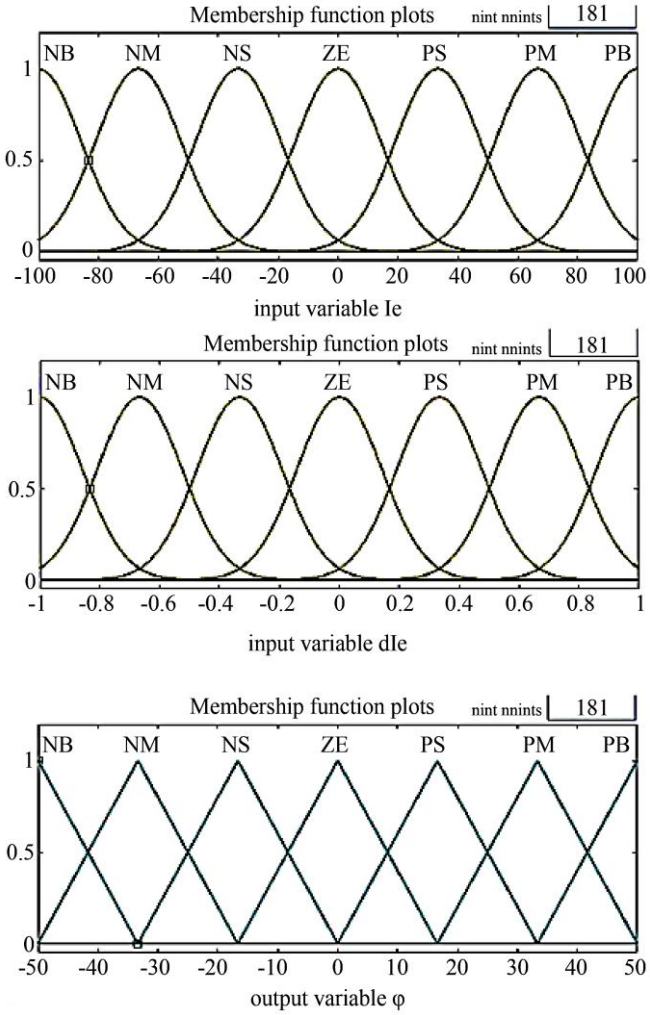

Fig. 5 Membership functions of input and output variables

3.2. ANFIS (Adaptive-Neuro Fuzzy Inference System) Controller

To further improve the FIS structure, the membership functions are trained using an optimization technique. The ANFIS tool available in MATLAB software is used for tuning the membership functions. The training data used for this purpose is imported from the PI controller module [21], while the PI controller module generates the input and output variables for the training. In the ANFIS control module, the input variable considered is the error current (Ie), while the output variable is the phase shift angle (φ). The structure considered is the 'Sugeno' type, with the output taken as constant values [22].

The input variable ranges between -100 to 100, similar to the FIS controller module. The membership functions of the input and output variables are set as per the response of the circuit topology. The input membership functions in ANFIS are maintained as a 'gauss' type, while the output membership functions are considered as constants [23]. The names of the membership functions are similar to those in the FIS module.

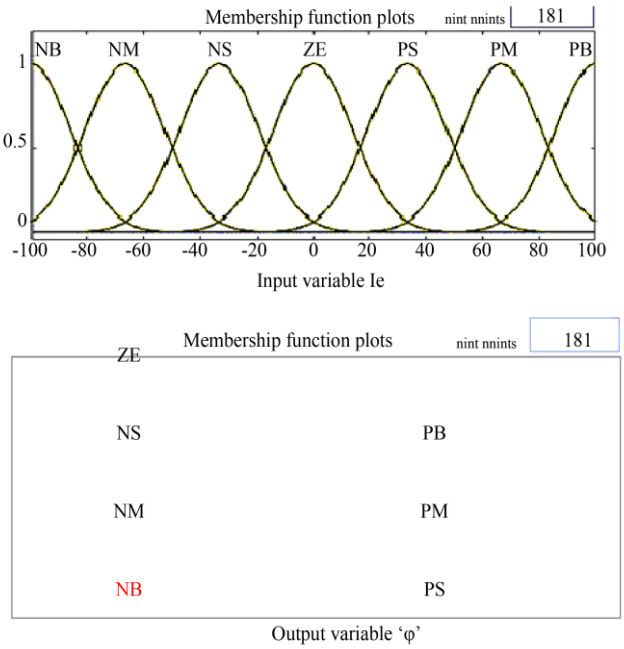

Fig. 6 ANFIS input and output variables

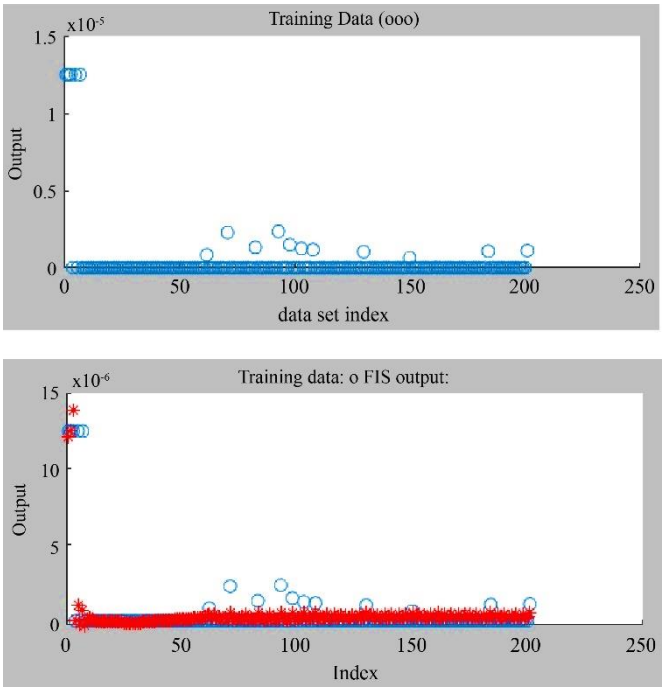

Fig. 7 Imported and trained data in the ANFIS tool

However, unlike in FIS, the rule table is not considered in ANFIS. Instead, a linear rule base is used. If Ie is NB, then φ is NB; If Ie is NM, then φ is NM; if Ie is NS, then φ is NS; if Ie is ZE, then φ is ZE; if Ie is PS, then φ is PS; if Ie is PM then φ is PM, If Ie is PB then φ is PB [24]. With this rule base, the ANFIS membership functions are trained from the input and output data imported from the PI controller. The data and training 'epchos' for the given system can be seen in Figure 7.

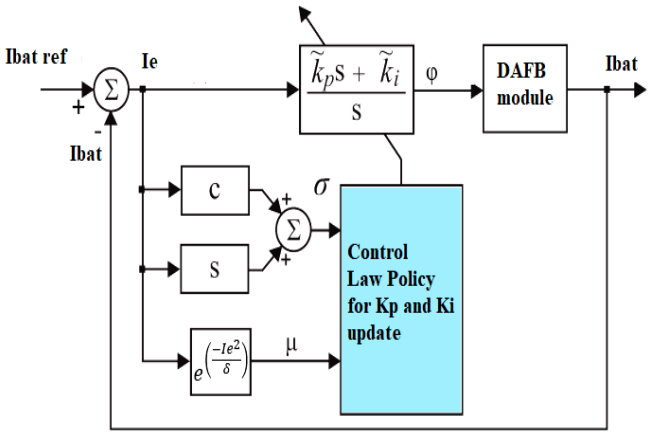

Fig. 8 DSM-PI controller design

Based on the figure presented above, the data imported from the PI control module undergoes training by using the 'hybrid' optimization algorithm available in the ANFIS tool with 100 epochs. This helps to achieve a precise output and reduced error coefficient. To carry out the training, 200 samples from the PI control module are considered for the training of the Sugeno file. The updated trained data is then used to update the membership functions with new ranges, which improves the response time of the system.

3.3. DSM-PI (Dual Sliding Mode – PI) Controller

The Dual Sliding Mode-PI controller is an improved version of the traditional PI control. It can adjust the Proportional (Kp) and Integral (Ki) gains according to the current error (Ie) [25]. The control module of PI is updated with a control law policy that updates the Kp and Ki values based on the error generated by comparing the reference and measured current [26] [17]. The DSM-PI controller design can be seen in Figure 8.

As per the above-given figure, the control law policy [25] depends on variables 'σ' and 'μ'. These variables are given as

$$\sigma = I_e.c + I_e s \tag{4}$$

$$\mu = e^{\left(\frac{-Ie^2}{\delta}\right)} \tag{5}$$

From these variables (4) and (5), the new Kp and Ki values are updated as per (6) and (7)

$$K_p = [(1 + sign(\sigma)K_p^+ - (1 - sign(\sigma))K_p^-] + K_p^{avrg} \tag{6}$$

$$K_i = [(1 + sign(\sigma)K_i^+ - (1 - sign(\sigma))K_i^-] + K_i^{avrg} \tag{7}$$

Table 2. DSM-PI controller constants

K_p^+=0.01	K_p^-=0.005	K_p^{avrg}=0.1
K_i^+=0.000012	K_i^-=0.00045	K_i^{avrg}=0.00023
c=100, s=2	δ = 500	μ =0.98

Table 3. System parameters

Parameters	Values
Grid	100MVA, 11kV, 50Hz
PV module	V_{mp} = 54.7V, I_{mp} = 5.58A, V_{oc} = 64.2V, 5.96A, N_p = 24, N_s = 7, $P_{pv\ opt}$ = 51kW.
Boost converter	R_b = 0.005Ω, L_b = 5mH, C_{out} = 12mF, f_{sw} = 5kHz.
β-MPPT	D_{int} = 0.5, β_{min} = -6500, β_{max} = -5400, β_g = -6000, MPPT gain = 5,
SRF controller	DC regulator gains: Kp = 7, Ki = 800 AC regulator gains: Kp = 0.3, Ki = 20 Vdc ref = 500V, Switching frequency = 1650Hz.
DAFB module	HFTF winding ratio- 1:1, $I_{bat\ ref}$ = 100A, High switching frequency = 20kHz, Phase shift regulator gains: Kp=0.1x10^{-6}, Ki = 5x10^{-9}.
Electric vehicle battery	Type: Lithium Ion, P_{nom} = 30kWh, V_{nom} = 320V, Capacity = 94Ah.

The gain values and the constant values for the given system are tuned and are set as per Table 2. In order to assess the controllers' robustness and their impact on battery current, the DAFB is controlled with various operating conditions and reference set points using control modules. The subsequent section includes a simulation and analysis of the entire system with all control modules, as well as a comparison of results and tables.

4. Results and Discussion

The Simulink software of MATLAB is used to model the given configuration of a test system that includes a PV source, an EV charging station, and a DAFB topology. The PV source is connected to the DC link through a boost converter that is controlled using the β-MPPT technique.

A 3-phase VSC controlled by the SRF method is connected to exchange power between the grid and the charging station. The EV charging station uses renewable power as per availability, and in case of PV source failure, it consumes power from the main grid. The modeling is as per the parameters given in Table 3.

For the simulation, the 'Powersystem' block sets from the Simulink library browser were used with the given parameters. All passive and active elements were set according to the system's specifications, and different operating conditions were simulated.

The analysis mainly focused on V2G and G2V conditions. The reference battery current was varied over time to validate the dynamic performance of the DAFB topology. Results were generated for different controllers in the PSPM control structure, including PI, FIS, ANFIS, and DSM-PI controllers.

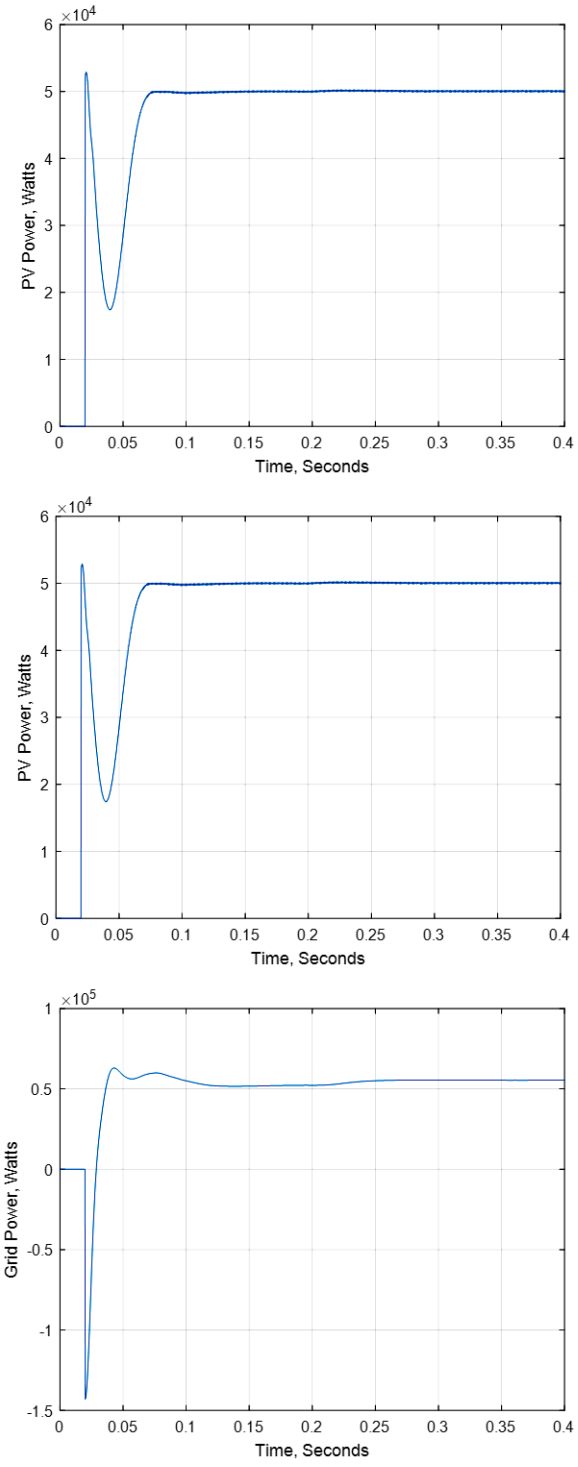

Fig. 9 Active powers of all modules (PV source, Grid and DAFB) during V2G operating mode

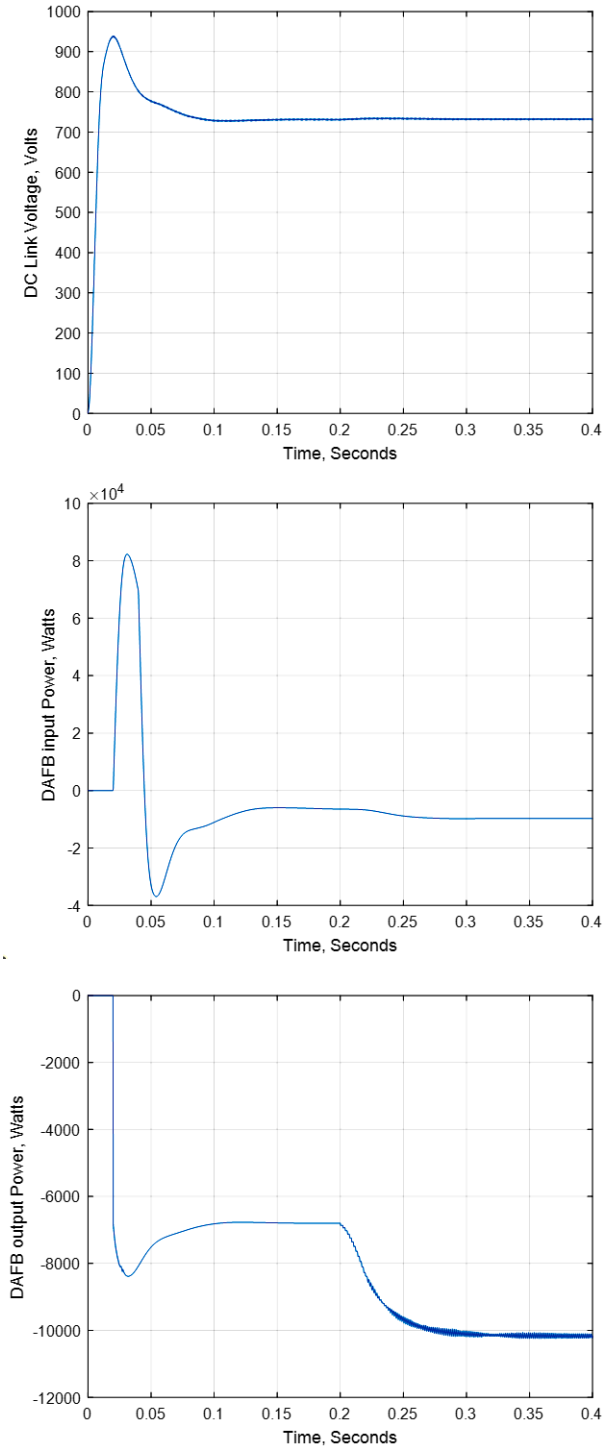

Fig. 10 DC link voltage, input, and output active powers of DAFB module during V2G operating mode

The simulation was run for 0.4 seconds, with the initial battery reference current set at 20A, which was later increased to 30A at 0.2 seconds. The graphical plots below show the results for different parameters of the system.

4.1. Vehicle to Grid (V2G) Condition

During this condition, the Electric Vehicle (EV) battery is discharged to the grid with a specific current reference of 20A from 0-0.2 seconds and then varied to 30A from 0.2-0.4 seconds. Figure 9 shows the active powers of the photovoltaic (PV) source, grid, and DAFB module for the given references.

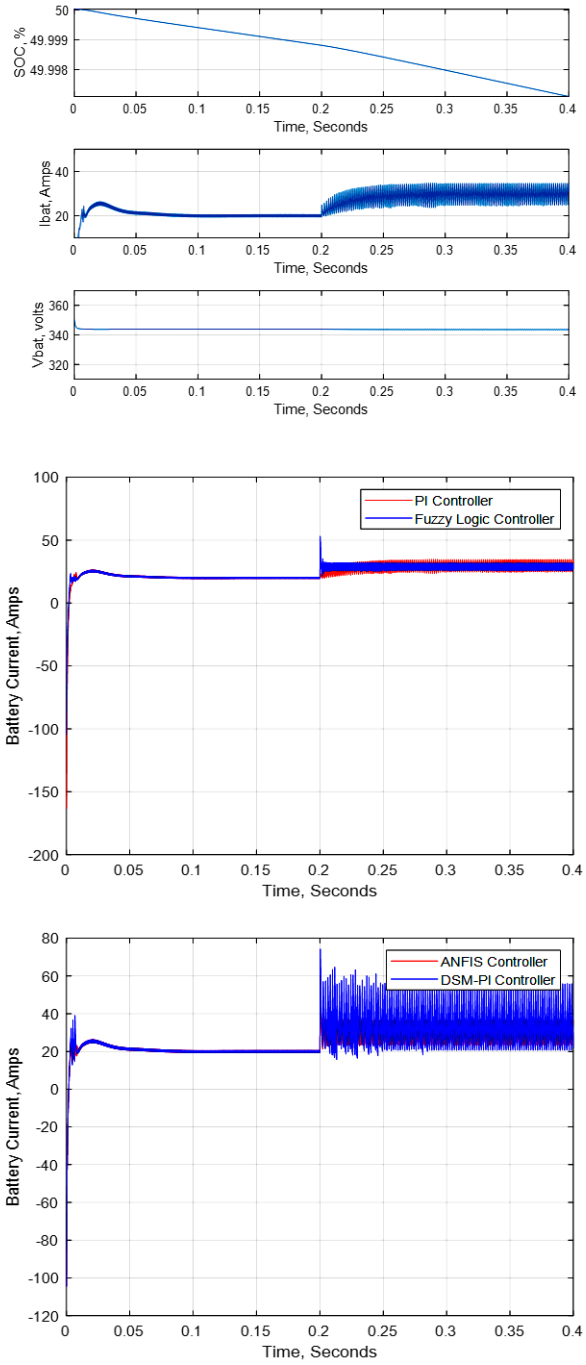

Fig. 11 Battery characteristics and battery current comparison during V2G operating mode

The solar irradiation remains constant at 1000W/mt2, generating solar power of 50kW, which is shared with the grid. From 0-0.2 seconds, the DAFB module also injects 6kW of EV power into the grid, making the total power injected into the grid 52kW (excluding losses). At 0.2-0.4 seconds, when the reference battery current is changed to 30A, the EV battery discharge is increased to 9.8kW, which is added to the grid, accumulating to 55kW injected into the grid.

According to the given conditions, the DC link voltage of the DAFB module remains at 722V even when the Ibat ref changes. In Figure 10, between 0-0.2 seconds, the total power drawn from the battery (Pin DAFB) is 6.6 kW, with a conversion loss of the DAFB module. This transferred power (Pout DAFB) to VSC is 6 kW. Between 0.2 and 0.4 seconds, the power drawn from the battery is 10.3 kW, and the power delivered to VSC by DAFB is 9.7 kW.

Figure 11 illustrates the battery behavior in V2G mode while utilizing different reference set points for battery discharge current. The EV battery's initial SOC (State of Charge) is set at 50%. The battery's positive side current measurement represents the discharge of the EV battery, which results in a decrease in SOC.

Figure 11 provides a comparison of battery current in V2G mode. The ANFIS module offers a more stable current with reduced ripple and accurate reference value generation. In the V2G condition, the ANFIS controller generates lower peak values during the initial state and at the variable reference state. Table 4 presents a parametric comparison of the V2G condition.

4.2. Grid to Vehicle (G2V) Operating Mode

During this mode of operation, the EV battery is charged while the DAFB consumes power from either the PV source or the grid. Figure 12 shows that the PV power remains constant at 50kW as there is no change in solar irradiation; however, the grid power and DAFB power change. At the beginning, from 0 to 0.2 seconds, the power shared to the grid is 38kW, which is the remaining power (excluding power loss) after 7.4kW of power is consumed by the DAFB module. From 0.2 to 0.4 seconds, the PV power shared to the grid decreases to 35kW as the DAFB module increases the reference set point to 30A, causing it to consume 10.3kW of PV power.

In the G2V operating mode, the DC link voltage is consistently maintained at 722V regardless of the reference set points. Based on Figure 13, from 0-0.2 seconds, the DAFB module receives 7.4kW of power from the PV source and delivers 6.8kW of power to the EV battery. From 0.2-0.4 seconds, the DAFB module receives 11kW of power and delivers 10.3kW of power to the EV battery. The difference between the input and output power of the DAFB module indicates that there is a loss of approximately 700W.

Table 4. Ibat Comparative analysis for V2G operating mode

	PI	FUZZY	DSM-PI	ANFIS
Initial peak value	27A	25A	25A	24A
Peak value	34	50	54	30
Settling time	0.12Sec	0.06Sec	0.06Sec	0.06Sec
Ripple %	13.50%	11.30%	9.80%	4.90%
Actual value generation	30A	29A	30A	30A

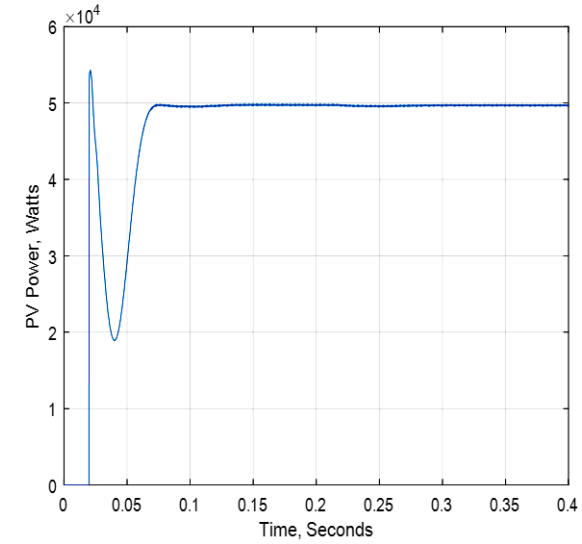

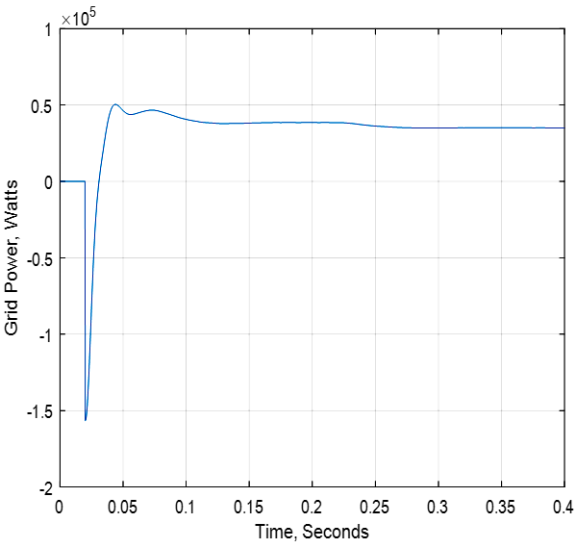

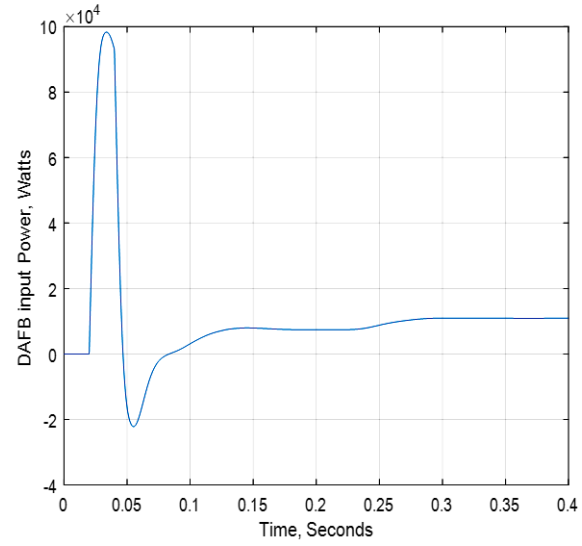

Fig. 12 Active powers of all modules (PV source, Grid and DAFB) connected at PCC during G2V operating mode

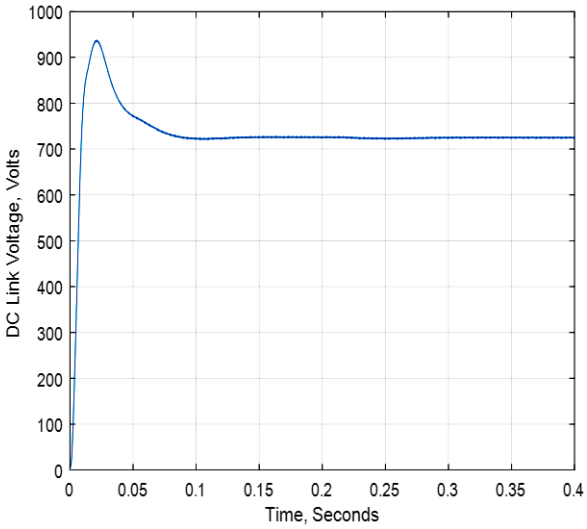

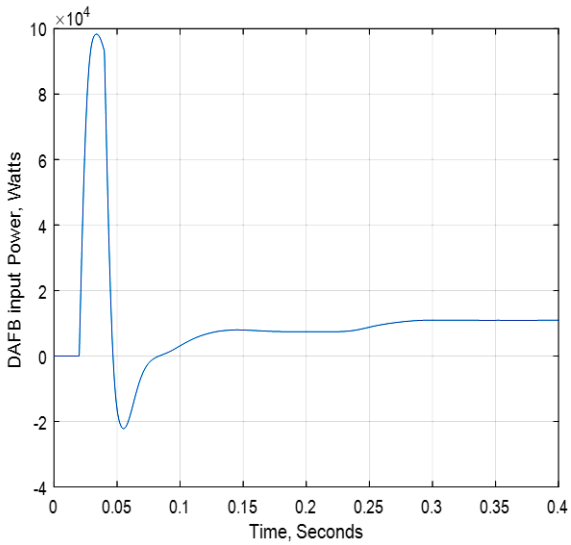

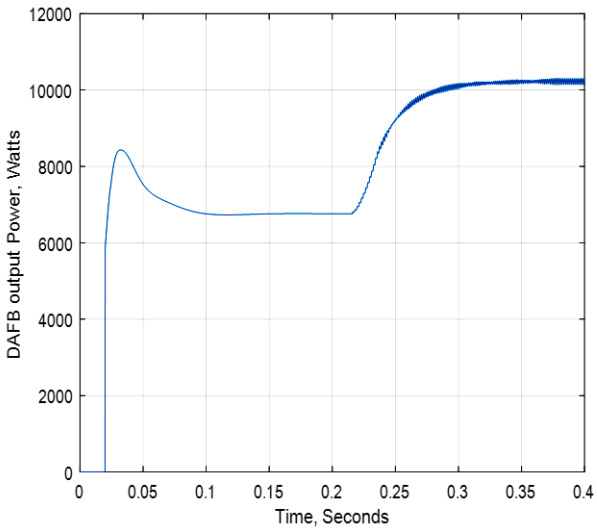

Fig. 13 DC link voltage, input and output active powers of DAFB module during G2V operating mode

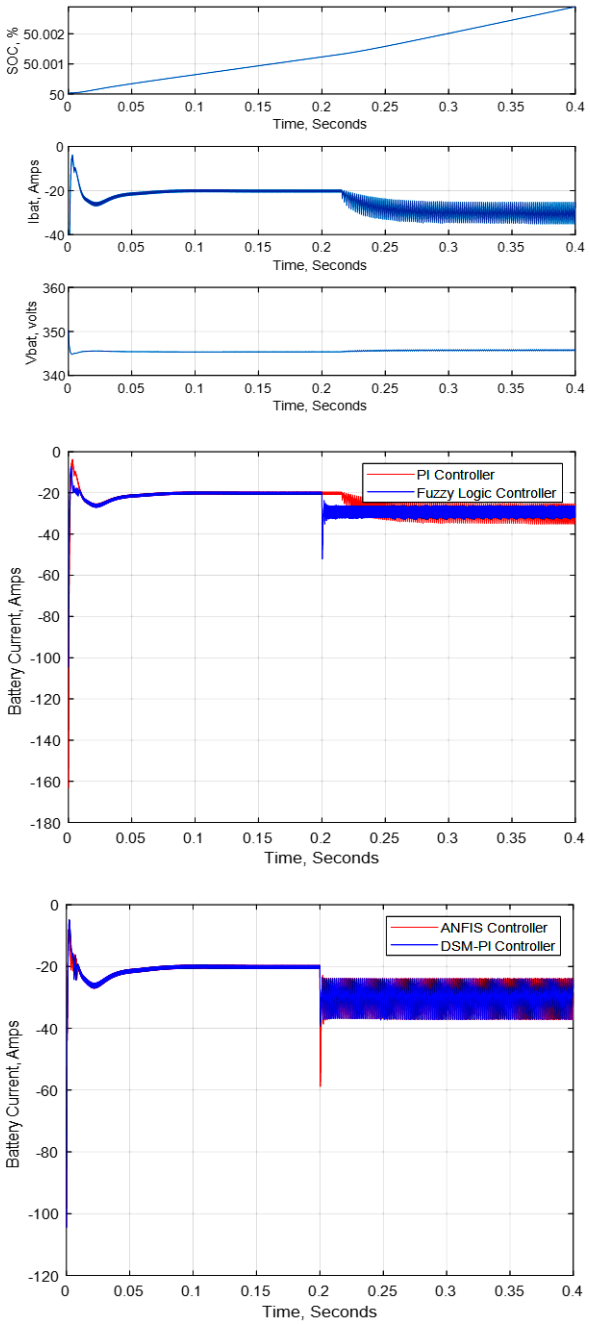

Fig. 14 Battery characteristics and battery current comparison during G2V operating mode

Table 5. Ibat Comparative analysis for G2V operating mode

	PI	FIS	DSM-PI	ANFIS
Initial peak value	-27A	-26A	-26A	-25A
Peak value	-34	-55	-60	-30
Settling time	0.1Sec	0.06Sec	0.06Sec	0.06Sec
Ripple %	11.50%	10.40%	8.50%	4.50%
Actual value generation	-30A	-29A	-30A	-30A

Figure 14 shows the characteristics of the EV battery during DAFB operation in G2V mode. Based on the comparison of battery current, the ANFIS controller demonstrates less ripple and faster response time. Additionally, the ANFIS control module generates reduced peak values, making it the better choice for controlling the DAFB module.

Table 5 compares the charging current (Ibat) of batteries controlled by different controllers, as the current varies between 20A and 30A.

5. Conclusion

The test system proposed for renewable power sharing to the grid and EV battery charging station has been implemented successfully. The EV charging station is equipped with a DAFB module for bidirectional power exchange from the EV battery to the grid.

The analysis of the DAFB module with G2V and V2G operating modes has been achieved using the PSPM technique. The PSPM technique has been updated with different controllers to improve the performance of the converter topology.

After a comparative analysis of PI, FIS, ANFIS, and DSM-PI control modules in the PSPM technique, it was found that the EV battery current is more stable and has reduced ripple content when operated with the optimized ANFIS controller. The settling time, actual value generation, and ripple factor of the EV battery current show.

References

[1] Mehrdad Ehsani et al., "State of the Art and Trends in Electric and Hybrid Electric Vehicles," *Proceedings of the IEEE*, vol. 109, no. 6, pp. 967-984, 2021. [CrossRef] [Google Scholar] [Publisher Link]

[2] Iqbal Husain et al., "Electric Drive Technology Trends, Challenges, and Opportunities for Future Electric Vehicles," *Proceedings of the IEEE*, vol. 109, no. 6, pp. 1039-1059, 2021. [CrossRef] [Google Scholar] [Publisher Link]

[3] Mohammad Esmaeili et al., "On the Role of Renewable Energy Policies and Electric Vehicle Deployment Incentives for a Greener Sector Coupling," *IEEE Access*, vol. 10, pp. 53873-53893, 2022. [CrossRef] [Google Scholar] [Publisher Link]

[4] Christopher H.T. Lee et al., "A Critical Review of Emerging Technologies for Electric and Hybrid Vehicles," *IEEE Open Journal of Vehicular Technology*, vol. 2, pp. 471-485, 2021. [CrossRef] [Google Scholar] [Publisher Link]

[5] Ante Lasić et al., "Supercapacitor Stack Active Voltage Balancing Circuit Based on Dual Active Full Bridge Converter with Selective Low Voltage Side," *2020 IEEE 11th International Symposium on Power Electronics for Distributed Generation Systems (PEDG)*, Dubrovnik, Croatia, pp. 627-636, 2020. [CrossRef] [Google Scholar] [Publisher Link]

[6] Junyun Deng, and Haoyu Wang, "A Hybrid-Bridge and Hybrid Modulation-Based Dual-Active-Bridge Converter Adapted to Wide Voltage Range," *IEEE Journal of Emerging and Selected Topics in Power Electronics*, vol. 9, no. 1, pp. 910-920, 2021. [CrossRef] [Google Scholar] [Publisher Link]

[7] Ujjwal Datta, Akhtar Kalam, and Juan Shi, *The Strategies of EV Charge/Discharge Management in Smart Grid Vehicle-to Everything (V2X) Communication Networks*, Advanced Communication and Control Methods for Future Smartgrids, pp. 1-21, 2019. [CrossRef] [Google Scholar] [Publisher Link]

[8] Prateek Jain, and Trapti Jain, "Application of V2G and G2V Coordination of Aggregated Electric Vehicle Resource in Load Levelling," *International Journal of Emerging Electric Power Systems*, vol. 19, no. 2, 2018. [CrossRef] [Google Scholar] [Publisher Link]

[9] Mahdi Shafaati Shemami et al., "Adaptive Neuro-Fuzzy Inference System (ANFIS) for Optimization of Solar Based Electric Vehicle-to-Home (V2H) Fuzzy Inference System (FIS) Controller," *2019 IEEE Transportation Electrification Conference and Expo (ITEC)*, Detroit, MI, USA, pp. 1-6, 2019. [CrossRef] [Google Scholar] [Publisher Link]

[10] Arnau Dòria-Cerezo et al., "Comparison of First- and Second-Order Sliding-Mode Controllers for a DC-DC Dual Active Bridge," *IEEE Access*, vol. 10, pp. 40264-40272, 2022. [CrossRef] [Google Scholar] [Publisher Link]

[11] Zhiqiang Guo, and Deshang Sha, "Dual-Active-Bridge Converter with Parallel-Connected Full Bridges in Low-Voltage Side for ZVS by Using Auxiliary Coupling Inductor," *IEEE Transactions on Industrial Electronics*, vol. 66, no. 9, pp. 6856-6866, 2019. [CrossRef] [Google Scholar] [Publisher Link]

[12] Suyash Sushilkumar Shah, and Subhashish Bhattacharya, "A Simple Unified Model for Generic Operation of Dual Active Bridge Converter," *IEEE Transactions on Industrial Electronics*, vol. 66, no. 5, pp. 3486-3495, 2019. [CrossRef] [Google Scholar] [Publisher Link]

[13] Satarupa Bal et al., "Improved Modulation Strategy Using Dual Phase Shift Modulation for Active Commutated Current-Fed Dual Active Bridge," *IEEE Transactions on Power Electronics*, vol. 33, no. 9, pp. 7359-7375, 2018. [CrossRef] [Google Scholar] [Publisher Link]

[14] Olympio Cipriano da Silva Filho et al., "Single-Phase Isolated AC-AC Converters Based on the Dual Active Bridge Converter," *IEEE Transactions on Industrial Electronics*, vol. 69, no. 6, pp. 5680-5689, 2022. [CrossRef] [Google Scholar] [Publisher Link]

[15] Amit Kumar Bhattacharjee, and Issa Batarseh, "An Interleaved Boost and Dual Active Bridge-Based Single-Stage Three-Port DC–DC–AC Converter With Sine PWM Modulation," *IEEE Transactions on Industrial Electronics*, vol. 68, no. 6, pp. 4790-4800, 2021. [CrossRef] [Google Scholar] [Publisher Link]

[16] Deliang Chen et al., "A Dual-Transformer-Based Hybrid Dual Active Bridge Converter for Plug-in Electric Vehicle Charging to Cope With Wide Load Voltages," *IEEE Transactions on Industrial Electronics*, vol. 70, no. 2, pp. 1444-1454, 2023. [CrossRef] [Google Scholar] [Publisher Link]

[17] Liang Guo, Yigeng Huangfu, and Yuxiang Zhang, "A Smooth Sliding Mode Control for a High-Conversion-Ratio Bidirectional DC-DC Converter," *2019 IEEE International Conference on Industrial Technology (ICIT)*, Melbourne, VIC, Australia, pp. 1669-1674, 2019. [CrossRef] [Google Scholar] [Publisher Link]

[18] Yudi Xiao et al., "A Universal Power Flow Model for Dual Active Bridge-Based Converters with Phase Shift Modulation," *IEEE Transactions on Power Electronics*, vol. 36, no. 6, pp. 6480-6500, 2021. [CrossRef] [Google Scholar] [Publisher Link]

[19] Rahmi İlker Kayaalp, Tuğçe Demirdelen, and Mehmet Tümay, "A Novel Fuzzy Logic Control for Bidirectional DC-DC Converter and Comparison with Dual Phase-Shift Control Method in Medium Voltage Applications," 2016 *IEEE International Conference on Computational Intelligence and Virtual Environments for Measurement Systems and Applications (CIVEMSA)*, Budapest, Hungary, pp. 1-6, 2016. [CrossRef] [Google Scholar] [Publisher Link]

[20] Nishit Tiwary et al., "Fuzzy Logic Based Direct Power Control of Dual Active Bridge Converter," *2021 1st International Conference on Power Electronics and Energy (ICPEE)*, Bhubaneswar, India, pp. 1-5, 2021. [CrossRef] [Google Scholar] [Publisher Link]

[21] Dante J.S. Oncoy, Rodrigo Cardim, and Marcelo C.M Teixeira, "Switched Control Based on Takagi-Sugeno Fuzzy Model for Dual Active Bridge DC-DC Converter," *2022 IEEE International Conference on Fuzzy Systems (FUZZ-IEEE)*, Padua, Italy, pp. 1-7, 2022. [CrossRef] [Google Scholar] [Publisher Link]

[22] Subhash Kumar Ram et al., "Analysis of Interleaved DC-DC Converter using ANFIS Control for EV Charging Applications," *2021 6th International Conference on Inventive Computation Technologies (ICICT)*, Coimbatore, India, pp. 374-378, 2021. [CrossRef] [Google Scholar] [Publisher Link]

[23] Sumana Ghosh et al., "Control of Grid-tied Dual-PV LLC Converter using Adaptive Neuro Fuzzy Interface System (ANFIS)," *IECON 2021 - 47th Annual Conference of the IEEE Industrial Electronics Society*, Toronto, ON, Canada, pp. 1-6, 2021. [CrossRef] [Google Scholar] [Publisher Link]

[24] K. Jyotheeswara Reddy, and N. Sudhakar, "High Voltage Gain Switched Capacitor Boost Converter with ANFIS Controller for Fuel Cell Electric Vehicle Applications," *2018 2nd IEEE International Conference on Power Electronics, Intelligent Control and Energy Systems (ICPEICES)*, Delhi, India, pp. 465-470, 2018. [CrossRef] [Google Scholar] [Publisher Link]

[25] Ricardo Lúcio de Araujo Ribeiro et al., "A Robust DC-Link Voltage Control Strategy to Enhance the Performance of Shunt Active Power Filters Without Harmonic Detection Schemes," *IEEE Transactions on Industrial Electronics*, vol. 62, no. 2, pp. 803-813, 2015. [CrossRef] [Google Scholar] [Publisher Link]

[26] Daniel O. Garrido et al., "Sliding Mode Control of Dual Active Bridge Converter with Resistive and Constant Power Load," *2022 IEEE Biennial Congress of Argentina (ARGENCON)*, San Juan, Argentina, pp. 1-8, 2022. [CrossRef] [Google Scholar] [Publisher Link]